SOLUTION MINING RESEARCH INSTITUTE
679 Plank Road
Clifton Park, NY 12065, USA

Telephone: +1 518-579-6587
www.solutionmining.org

Technical Conference Paper

1965 – 2025

Hydrogen Storage Favorability Analysis for the Aptian Evaporites in the Alagoas Basin, NE Brazil

Flavio Botelho, Federal University of Pernambuco, Recife, Brazil

José Antonio Barbosa, Federal University of Pernambuco, Recife, Brazil

Jefferson Oliveira, Federal University of Pernambuco, Recife, Brazil

Osvaldo Correia, Federal University of Pernambuco, Recife, Brazil

SMRI Fall 2025 Technical Conference
29-30 September 2025
Wichita, Kansas, United States

Solution Mining Research Institute Fall 2025 Technical Conference

Wichita, Kansas, United States 29-30 September 2025

Hydrogen Storage Favorability Analysis for the Aptian Evaporites in the Alagoas Basin, NE Brazil

Flávio Botelho, Federal University of Pernambuco, Recife, Brazil

José Antonio Barbosa, Federal University of Pernambuco, Recife, Brazil

Jefferson Oliveira, Federal University of Pernambuco, Recife, Brazil

Osvaldo Correia, Federal University of Pernambuco, Recife, Brazil

Abstract

The Aptian Paripueira evaporites of the Maceió Formation, deposited during the rift phase of the Alagoas Basin in northeastern Brazil, represent a significant, yet underexplored, opportunity for large-scale geological energy storage. These evaporite deposits occur as a sequence of at least four distinct cycles covering an area of approximately 200 km² (77.2 sq mi). These salt beds are locally folded and tilted by halokinetic deformation and rift-related faults. The evaporitic succession also presents high-frequency interlayers of insoluble layers, which pose geomechanical challenges for the development of energy storage projects. Despite the potential opportunity, the complex tectono-structural framework involving these evaporitic deposits requires a detailed characterization to ensure the technical success of potential storage projects based on the construction of artificial caves. This study presents a comprehensive assessment of the suitability of these salt deposits for developing hydrogen storage in artificial caves.

To address these complexities, a multi-source dataset, including 15 wells, 15 2D seismic sections, a 3D seismic cube, and a gravimetric survey, was integrated to build a 3D tectono-stratigraphic model. Geostatistical analysis was applied to produce geomodels considering key engineering and geological parameters. These included depth to the top of the evaporitic succession, evaporitic beds thickness, percentage of insoluble materials, quantity and thickness of interlayers, and the distance to the border of the evaporitic basin. The geometry of the main faults was discretized for modeling. After the modeling, the parameterized grids were cross-correlated through a scoring methodology to produce comprehensive favorability maps, highlighting areas with the most suitable conditions for cavern construction.

The research products provided a thorough guide to mitigate future investment risks. Despite the inherent geological complexities, the analysis identified favorable zones that support the allocation of a conceptual field with 237 caverns. This configuration yields a total effective energy storage potential of approximately 13.5 TWh, establishing the area as a strategic asset for a potential regional hydrogen hub in northeastern Brazil. This region presents enormous potential for green hydrogen production due to the immense availability of renewable energy, which reinforces the strategic importance of evaporite deposits studied here. It must be noted, however, that this assessment is conceptual, and a definitive allocation of the number and capacity of caverns is contingent upon corroboration from detailed field investigations, including dedicated drilling and specific engineering design.

Key words: Hydrogen storage, De-risk analysis, Tectono-stratigraphic modeling, Geostatistical modeling, Paripueira Evaporites, Geological screening.

1. Introduction

The global energy transition towards a climate-neutral economy is critically dependent on the large-scale integration of renewable energy sources such as wind and solar power. However, the inherent intermittency of these sources creates a fundamental mismatch between energy supply and demand, implying the necessity of developing large-scale, long-duration energy storage solutions to ensure grid stability and reliability (Huang & Yin, 2025). Hydrogen is recognized as a key energy carrier poised to bridge this gap, offering a potential way to store and transport clean energy (Allsop et al., 2023). Geological storage is considered the most effective and viable pathway to achieve the gigawatt to terawatt-scale, inter-seasonal storage capacity required to support a future hydrogen economy (Duartey et al., 2025). Among the geological media used for gas storage, salt caverns stand out as the most mature and promising technology for underground hydrogen storage (UHS), leveraging decades of operational experience from the natural gas industry (Zhu et al., 2024; Oni et al., 2025). Salt caverns offer an attractive combination of high sealing capability due to the rock salt's low permeability, chemical inertness for hydrogen, large volume capacity, and the ability to sustain the fast, high-frequency injection and withdrawal cycles required to balance the grid (Allsop et al., 2023; Oni et al., 2025).

Brazil, with its predominantly renewable energy matrix, is strategically positioned to become a key player in the global green hydrogen economy (Rocha et al., 2012). The country's northeastern region, in particular, boasts exceptional natural endowments, including some of the world's highest-quality wind and solar resources, making it a prime candidate for large-scale green hydrogen production and a major competitor for international investments in the sector (Anjos et al., 2024). Located within this promising region (Fig. 1), the onshore portion of the Alagoas Basin hosts an extensive, yet largely unexplored, Aptian-age evaporitic succession known as the Paripueira Evaporites, which are part of the Maceió Formation (Martins et al., 2019). These salt deposits represent a significant strategic target for developing the large-scale UHS capacity required to anchor a regional hydrogen hub. However, the tectono-stratigraphic context of these deposits is complex, with multi-episode structural deformation involving halokinesis and rift-related faulting. Another complex factor is the occurrence of high frequency interlayers (Martins et al., 2019). This geological complexity presents considerable challenges to the construction and operation of salt caverns, regarding the required long-term stability and integrity aspects, which demands detailed investigations to assess its true potential for UHS projects (Oni et al., 2025; Zhang et al., 2017).

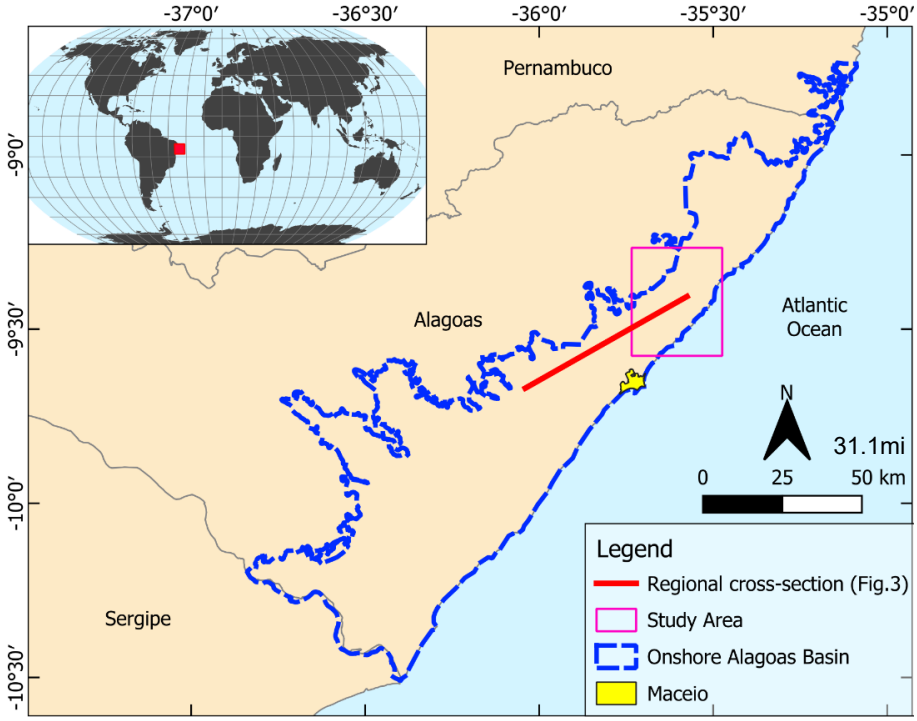

Fig. 1. Location of the study area in the northeast Brazil with state limits.

This study presents the first systematic and quantitative potential assessment of the Aptian evaporitic succession in the northern part of the onshore Alagoas Basin for developing UHS projects. The research aimed to use the available public geological and geophysical legacy data for a detailed de-risking analysis for the storage potential involving salt caves (Allsop et al., 2023; Zhu et al., 2024). The presented research aimed the characterization and ranking of the most promising areas for salt caverns development, to provide a strategic guide to optimize future capital-intensive exploration campaigns, pilot projects, or commercial projects in the region.

2. Geological Setting

2.1. Tectonic Evolution of the Alagoas Basin

The marginal Alagoas Basin holds a complete geological record of the tectonic processes associated with the fragmentation of the Gondwana supercontinent and the subsequent opening of the South Atlantic Ocean (Martins, 2016). Its formation is directly linked to the Early Cretaceous continental rift phase of Central South Atlantic (Kifumbi et al., 2017). The Mesozoic-Cenozoic stratigraphic record of the basin reflects four distinct tectonic phases: pre-rift, rift, post-rift (or transitional), and drift (Kifumbi et al., 2017). The rift stage, which occurred during the Early Cretaceous, was characterized by accentuated mechanical subsidence that created a complex system of grabens and half-grabens (Kifumbi et al., 2017).

The basin's structural architecture was dominated by an extensional regime trending NW-SE, whichcreated a dominant framework of NE-trending normal faults. The post-rift phase involved significantly less tectonic activity and led to the development of a broader, less compartmentalized basin (Caixeta et al., 2014). The Aptian evaporites were deposited precisely during this period when the basin was experiencing a quieter tectonic stage.

2.2. The Aptian Evaporitic Succession of the Fazenda Guindaste Low

The Aptian syn-rift succession of the Alagoas Basin is divided in three distinct evaporitic depositional periods, named Horizonte, Paripueira, and Ibura (Martins, 2016), from the oldest to the youngest. These events are positioned within the rift sequence of the basin (Fig. 2). While all three represent significant saline deposition, this study focuses specifically on the Paripueira evaporites, which are stratigraphically positioned within the Maceió Formation (Martins et al., 2019).

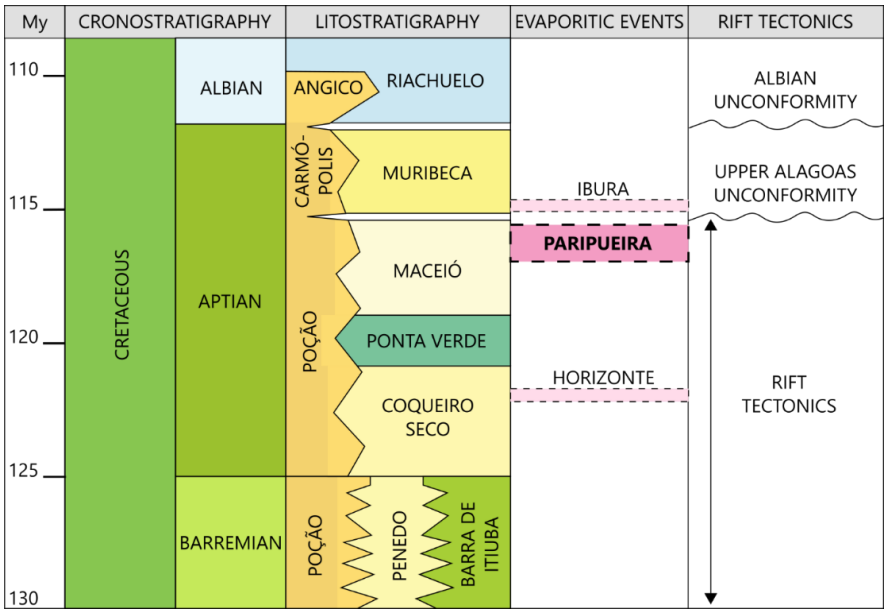

Fig. 2. Stratigraphic chart of the Alagoas Basin (Barremian-Albian) showing stages, stratigraphic units, evaporitic events, and the interpretation for the timing of rift tectonics. Modified from Martins et al. (2019), who compiled and modified data from Campos Neto et al. (2007), Cruz (2008), and Souza-Lima (2008).

The deposition of the Paripueira evaporites occurred in a restricted lacustrine environment (Martins, 2016). This geological period was marked by an arid climate, which, combined with the physiographic restriction imposed by active faulting, led to high evaporation rates that exceeded water influx (Florencio, 2001; Martins, 2016). These conditions led to the desiccation of the lakes and the consequent precipitation of thick salt layers (Martins, 2016). The occurrence of these deposits is confined to specific structural grabens that acted as isolated depocenters. The study area is located within one of these depocenters, the Fazenda Guindaste Low, an elongated graben controlled by a complex set of rift-related faults, including synthetic and antithetic normal faults, transfer zones, and rollover anticlines (Martins et al., 2019). Fig. 3 shows a regional geological section trending NE-SW, which shows the tectono-stratigraphic configuration of the two main grabens that dominate the onshore region. The stratigraphic position of the two main evaporitic successions is depicted. The Paripueira evaporitic deposits are positioned within the Maceió Formation in the Fazenda Guindaste Low.

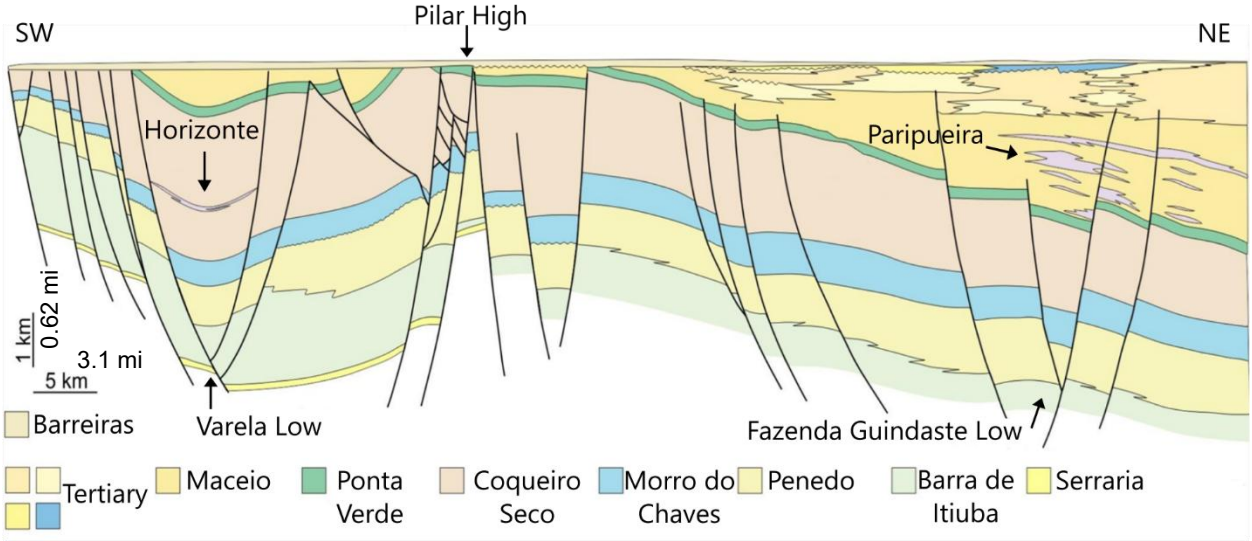

Fig. 3. Geological cross-section through the Alagoas Basin, cutting from the the area of the Varela Low to the Fazenda Guindaste Low, showing the Horizonte and Paripueira evaporites. Modified from Martins (2016), who adapted the original section from Souza-Lima (2008).

The Paripueira succession consists of thick layers of halite with a notable absence of anhydrite or more soluble potassium and magnesium salts (Florencio, 2001; Martins, 2016). The evaporitic succession is marked by a significant input of terrigenous sediments, represented by tens of interlayers composed of shales, carbonates, and shaly siltstones (Florencio, 2001; Souza-Lima et al., 2019). The sediments interbedded with the salt beds are frequently immature gravitational flow deposits, which provide evidence of syn-tectonic influence on the salt basin formation (Martins, 2016). The rift phase produced topographic restrictions that influenced the evaporitic deposition on the lacustrine depocenters (Martins et al., 2019).

3. Dataset and Methodology

We used a large public dataset to analyze the regional characteristics of the salt basin and help de-risk future UHS projects (Allsop et al., 2023). The first step was to integrate the available geological and geophysical data; a second step consisted of creating a detailed 3D model, which allowed a thorough tectono-stratigraphic interpretation of the basin´s region where the salt deposits formed during the end of the rift stage. In the third step, we performed an analysis based on geostatistical models, which provided a quantitative evaluation of the economic aspects of these deposits regarding the UHS application. A favorability algorithm was applied, which allowed us to verify the suitable areas for H2 storage, including the strategic allocation of salt caverns, and a preliminary estimation of the storage capacity.

The geological and geophysical data used represent legacy data from the oil industry, and were provided by the REATE Project, a consortium between the Brazilian Geological Survey (SGB) and the Brazilian National Agency of Petroleum, Natural Gas and Biofuels (ANP). The dataset includes 15 2D Seismic sections, one 3D time-migrated seismic volume, and data from 15 wells, including geological information and geophysical logs. We also used a gravimetric survey that covers most of the studied region to complement the regional tectono-stratigraphic framework.

3.1. Geological and Geophysical Dataset

Fifteen wells were selected to provide a detailed interpretation of the evaporitic succession, including the individualization of the deposition cycles, the average thickness of the main salt beds, and the syn-rift phase effect on the salt basin evolution. The wells were also used to delineate the areal extent of the salt basin. Fifteen 2D seismic sections were selected to build the 3D model, including the stratigraphic framework and the main faults. Furthermore, the 3D seismic cube was integrated into the 3D model to provide the delineation of some features like faults and folds over the northeast sector of the salt basin, where no wells have been drilled. The gravimetric data provided by the ANP was processed into a Residual Bouguer Anomaly map by using a 5-25 km (3.1-15.5 mi) band-pass filter (Medeiros et al., 2006).

Fig. 4 shows the location of geophysical data and wells used to investigate the study area, highlighting the regional characteristics of the depocenter: an elongated NE-SW trend bordered to the west by the crystalline basement and to the east by an external hinge of the basin.

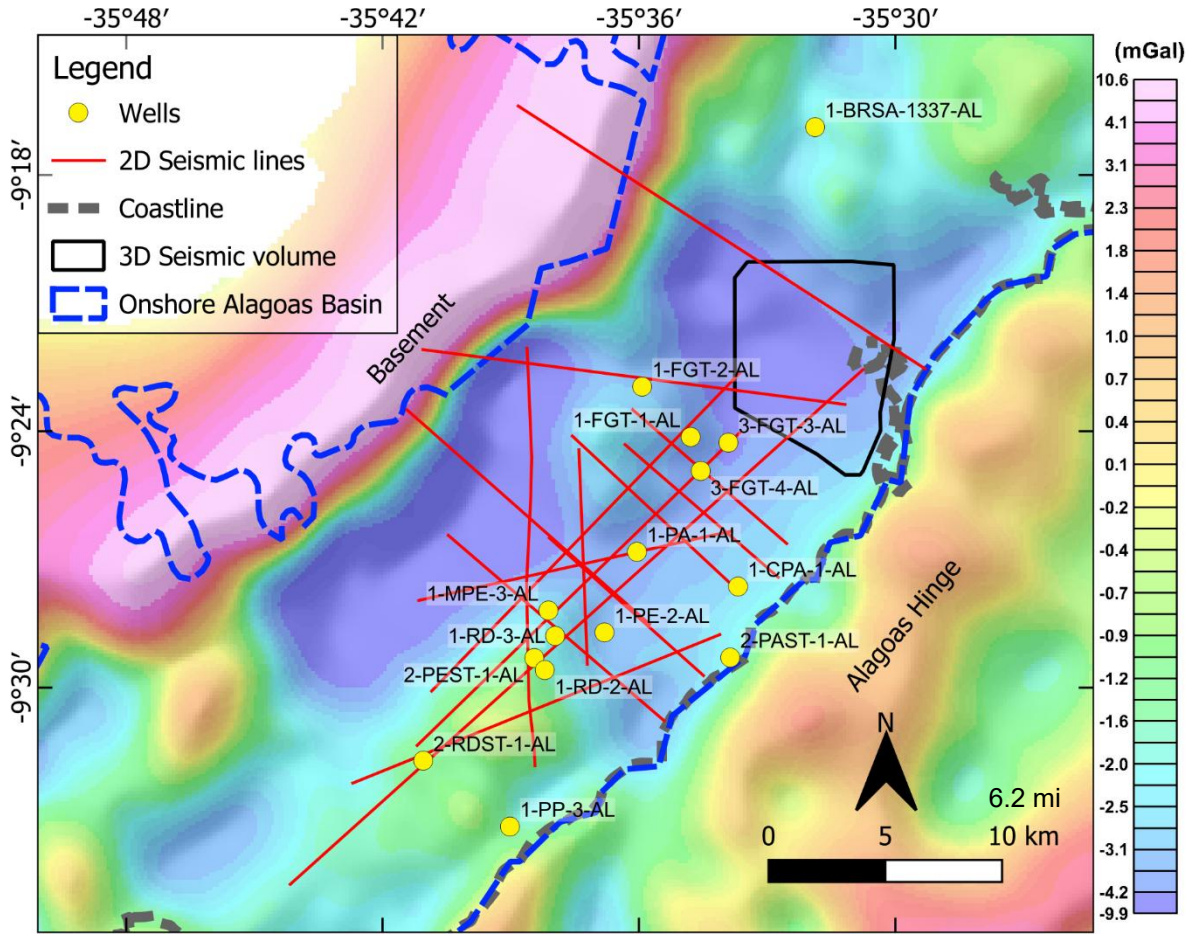

Fig. 4. Characteristics of the study area. The Residual Bouguer Anomaly Map (Medeiros et al., 2006) shows the main features of the basement. The 2D seismic sections and the boreholes are concentrated in the eastern part of the depocenter, and the 3D seismic cube is located in its northeast border.

3.2. 3D Tectono-Stratigraphic Modeling

We used Residual Bouguer anomaly map and the stratigraphic wells to interpret the regional tectonic framework. The interpretation of the stratigraphic successions was guided by well data, and horizons marking the top and base of the formations allowed the delineation of regional surfaces. The interval encompassing the salt deposits was divided into four main evaporitic cycles. These cycles were then discretized and modeled as 3D geobodies. For the time-to-depth conversion of the seismic data, a velocity model was generated from the sonic well log data that intersected the evaporitic cycles. This integrated interpretation allowed for the characterization of the subsurface architecture and the modeling of the two main fault systems that affected the salt beds: a system of deep-seated faults from the rift phase and a secondary shallower system of listric and detachment faults created by the salt tectonics (halokinesis). A schematic diagram of the modeling workflow is shown in Fig. 5.

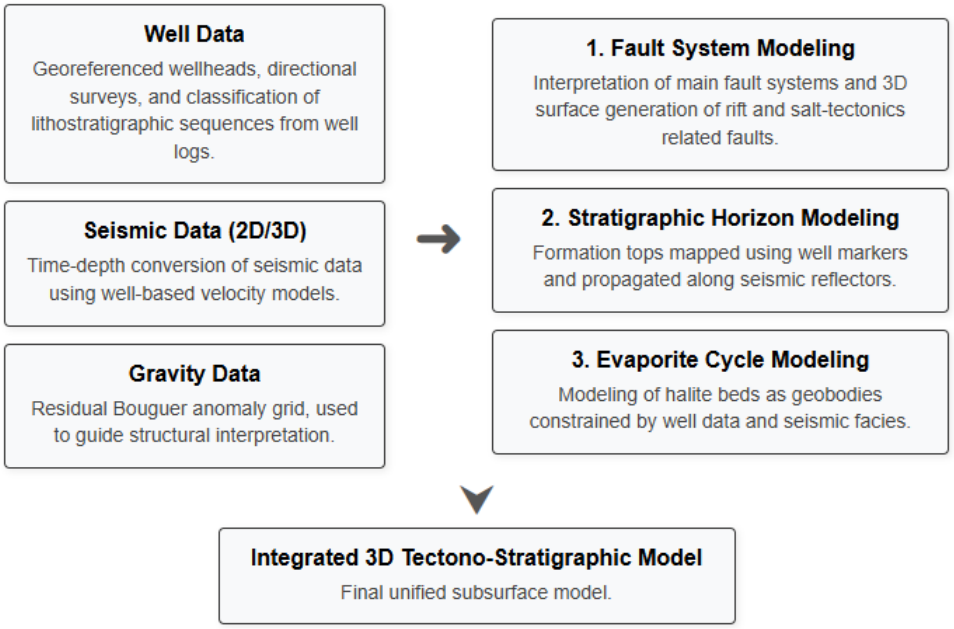

Fig. 5. Geological and geophysical data processing workflow. The methodology begins with the integration of well and seismic data in a 3D environment, which allows the building of the geological model. This is followed by (1) fault system modeling, (2) stratigraphic horizon mapping, and (3) evaporite cycles modeling.

3.3. Parameter Grid Generation and Favorability Algorithm.

To assess the suitability of the salt beds for UHS, we used a geostatistical approach, detailed in Fig. 6. The processing of the data was conducted by using a custom Python application implemented for this research. The code is based on a multi-parameter decision model for site selection (Zhu et al., 2024). The first step is the generation of spatial parameter grids, with a cell size of 50 x 50 m (164 x 164 ft), based on key geological and engineering criteria, such as salt thickness, fault proximity, and interlayer content (Allsop et al., 2023; Zhu et al., 2024). Geometric grids, such as depth to top and cycle thickness, were extracted from the 3D model. Other grids aimed to analyze the proximity factor between elements, including the distance to fault surfaces (calculated from the modelled 3D faults using a k-d tree algorithm) and the distance to the edge of the salt beds (calculated using a distance transform), were also created. Key rock property grids, including the percentage of insolubles and the quantity and maximum thickness of the interlayers were generated with the interpolation of the well-based stratigraphic data using the Inverse Distance Weighting (IDW) method.

A critical intermediate step was the calculation of a potential cavern volume grid. This was performed cell by cell, considering the local net salt thickness and a cavern design with a maximum diameter of 80 m (262 ft). The design aimed to fit a cavern with a height-to-diameter (H/D) ratio between 1.5 and 2.0, optimized for the available thickness, while reserving safety margins for the roof (hanging wall) and floor (footwall) of 75% and 20% of the diameter, respectively (Allsop et al., 2023, Huang & Yin 2025).

An algorithm was used to extract the favorability aspect. Each parameter treated was normalized from 0 (unfavorable/unviable) to 10 (highly favorable). These scored grids were then combined using a weighted overlay analysis. Thus, cutoff conditions were applied to define the limits of acceptance: if a critical parameter (e.g., depth, fault distance) fell outside its operational window (Allsop et al., 2023; Zhu et al., 2024), the final favorability score for that location is forced to zero. The parameters and thresholds used in the algorithm are detailed in Table 1.

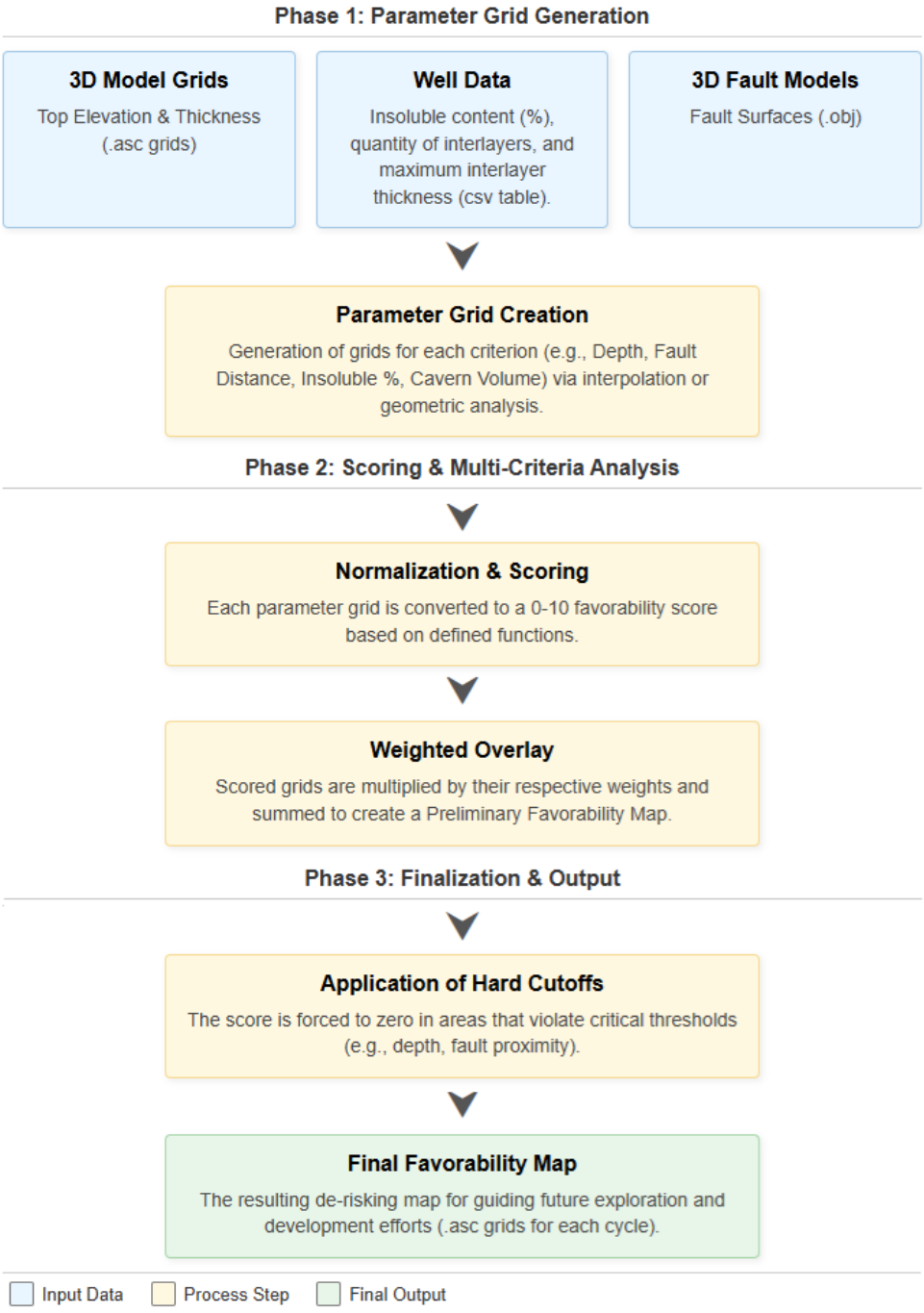

Fig. 6. Schematic description of the favorability mapping algorithm. The workflow is divided into three main stages: (1) generation of spatial parameter grids from various input data; (2) a multi-criteria analysis involving normalization, scoring, and a weighted overlay of the grids; and (3) the application of hard cutoffs to produce the final de-risking map.

Table 1. Summary of parameters and criteria used in the favorability mapping algorithm. The table details the scoring functions for each of the eight selected parameters, including the lower and upper cutoff values, the thresholds for the optimal score (10), and the methodology for score calculation in the intermediate range. Key literature supporting the chosen criteria and the final weights assigned to each parameter in the weighted overlay analysis are also listed.

Parameter	Lower Cutoff (Annulment/Min Score)	Upper Cutoff (Annulment/Max Score)	Score Range (Variable Favorability)	Main Reference (Support for Suggestion)	Weight
1. Depth to the top of the evaporitic cycle (m)	< 500m (1640ft) (Annulment, Score 0)	>2000m (6560ft) (Annulment, Score 0)	500m – 2000m (Score 0 at extremes, Gaussian optimum at 1250m (4100ft) ± 350m (1150ft))	Zhu et al. (2024); Allsop et al. (2023); Caglyan et al. (2020); Xia et al. (2017)	1.80
2. Evaporite cycle total thickness (m)	< 100m (328ft) (Annulment, Score 0)	N/A (Values >300m (984ft) receive Score 10)	<100m (score 0), >300m (score 10), linear	Huang & Yin (2025); Allsop et al. (2023)	1.40
3. Insoluble fraction of the cycle (%)	N/A (0% is ideal, Score 10)	N/A (Values >40% receive Score 0)	0% (score 10) to 40% (score > 0), linear	Huang & Yin (2025); Allsop et al. (2023)	1.00
4. Quantity of interlayers	N/A, (0 = Score 10)	N/A (>20 = Score 0)	0 (score 10); linear variation; 20 (score 0).	Huang & Yin (2025); Allsop et al. (2023); Yu et al. (2022)	1.00
5. Maximum thickness of interlayers in the cycle (m)	N/A, 0m (Score 10)	N/A (>30m (98ft) = score 0)	0m = score 10, >30m = score 0, linear	Huang & Yin (2025); Allsop et al. (2023); Yu et al. (2022)	1.00
6. Distance to main faults (3D model) (m)	≤ 100m (328ft) (Annulment, Score 0)	N/A (Values ≥500m (1640ft) receive Score 10)	>100m to <500m (Linear interpolation for score 0-10).	Zhu et al. (2024)	1.40
7. Distance of a given point to the evaporitic cycle perimeter edge	≤ 500m (1640ft) (Annulment, Score 0)	N/A (Values ≥2000m (6560ft) receive Score 10)	>500m to >2000m (Linear interpolation for score 0-10).	Zhu et al. (2024); Allsop et al. (2023); Yu et al. (2022)	1.40
8. Cave Volume (m^3)	< 100,000m^3 (3.53 MMcf) (Annulment, Score 0)	N/A (Values ≥400,000m^3 (14.12 MMcf) receive Score 10)	100000 m^3 ≤ volume < 400000m^3 (Linear interpolation for score 0-10).	Zhu et al. (2024); Allsop et al. (2023); Yu et al. (2022)	1.00

3.4. Preliminary Storage Capacity Estimation

The final stage of the methodology focused on estimating the studied region's hydrogen storage potential capacity. This was achieved by combining an algorithm used to locate the caverns with a sequential thermodynamic calculation used to determine operational storage capacity for each potential cavern.

First, a conceptual cavern field was defined. The optimal location of the caverns was achieved by using an algorithm written in Python, which placed the caverns following a defined threshold (e.g., score > 6). The location logic iteratively selects the highest-scoring available location and creates an exclusion zone around it, considering the geomechanical parameters. The acceptable pillar width between caverns was set to three times the cavern diameter, resulting in a center-to-center spacing of four times the cavern diameter, regarding a factor recommended to ensure the geomechanical safety (Caglayan et al., 2020; Allsop et al., 2023).

After achieving the best fit in terms of caverns distribution, the operational storage gas capacity for each unit was determined through a four-step thermodynamic calculation:

1. Determination of Cavern Conditions: The best reference depth for each cavern (D_{cavern}) was established at the midpoint of the salt cycle. This was calculated for each cavern's location by retrieving the depth of the cycle's top surface from the elevation grid and the cycle's total thickness from the thickness grid. The in-situ temperature (T_{cavern}) and lithostatic pressure (P_{sv}) were then calculated based on this reference depth:

$$T_{cavern}(K) = \left(T_{surface} + \left(\frac{D_{cavern}}{1000} \times \nabla T\right)\right) + 273.15 \quad (1)$$

$$P_{sv}(MPa) = \frac{\rho_{rock} \times g \times D_{cavern}}{1{,}000{,}000} \quad (2)$$

Where $T_{surface}$ is the average surface temperature, assumed as 25 °C (77 ºF), ∇T is the regional geothermal gradient, estimated at 25°C/km (13.7 ºF / 1000 ft) (Argollo et al., 2012), ρ_{rock} is the estimated average rock density of the overburden assumed as 2200kg/m³ (137.3 lb/ft³)(based on well logs), and g is the acceleration of gravity (9.8 m/s²) (32.2 ft/s²).

2. Operating Pressure Window: The maximum (P_{max}) and minimum (P_{min}) operating pressures were defined as fractions of the local lithostatic pressure, consistent with industry standards for ensuring cavern stability (Liu et al., 2024). The maximum pressure is limited to avoid tensile stress and fracturing of the salt, while the minimum pressure is required to counteract creep-induced convergence (Zhang et al., 2017; Allsop et al., 2023).

$$P_{max} = 0.80 \times P_{sv} \quad (3) \qquad P_{min} = 0.30 \times P_{sv} \quad (4)$$

3. Hydrogen Density Calculation: The hydrogen density (ρ_{H2}) at both P_{max} and P_{min} was then calculated. This first required determining the compressibility factor (Z) by using the standardized virial-type equation of state from Lemmon et al. (2008) (see Appendix A for coefficients):

$$Z = 1 + \sum_{i=1}^{9} A_i \cdot \left(\frac{P_{MPa}}{1}\right)^{B_i} \cdot \left(\frac{T_{cavern}}{100}\right)^{-C_i} \quad (5)$$

The density was then derived from the real gas law:

$$\rho_{H2} = \frac{P \times M_{H2}}{Z \times R \times T_{cavern}} \quad (6)$$

Where M_{H2} is the molar mass of H_2 (2.01588 g/mol), and R is the universal gas constant (8.314472 J/(mol·K)) (Lemmon et al., 2008).

4. Storage operational capacity and Energy Storage: Finally, the working gas mass ($M_{working}$) and the stored energy ($E_{effective}$) were estimated. The volume for each cavern (V_{cavern}) was sourced from the potential cavern volume grid (Section 3.3). This grid provides the effective useful volume, which has been adjusted not only regarding the safety distance limits but also for the sump volume occupied by accumulated

insoluble materials. The sump volume calculation considered the percentage of interlayers and a bulking factor of 1.3 to account for the expansion of this material at the cavern bottom. The working gas mass was calculated as the difference between the mass of hydrogen at maximum and minimum pressures (Allsop et al., 2023) (Equation 7). Subsequently, the gas mass was converted into an effective energy potential (Equation 8). This value represents the net electrical energy that could be generated from the working gas storage capacity in the caverns considered, assuming a specific power generation efficiency (η_{gen}) of 50%. This factor accounts for the thermodynamic and operational losses inherent in converting the chemical energy of the stored hydrogen to electricity, for instance, using a Combined Cycle Gas Turbine (CCGT) adapted for hydrogen (Harrison et al., 2010). The total storage potential was determined by summing the capacity of all caverns allocated in the evaporitic beds.

$$M_{working} = \left(\rho_{P_{max}} - \rho_{P_{min}}\right) \times V_{cavern} \quad (7)$$

$$E_{effective} = \frac{M_{working} \times LHV_{H2} \times \eta_{cycle}}{3.6 \times 10^9} \quad (8)$$

Where LHV_{H2} is the Lower Heating Value of hydrogen (120 MJ/kg) and η_{gen} is the power generation efficiency (50%), representing the conversion factor from the chemical energy of the working gas to the net electrical output.

4. Results

4.1. The Tectono-Stratigraphic Framework

The interpretation of the wells and seismic data led to the creation of a surface related to the top of the Coqueiro Seco Formation. This surface represents the base of the evaporitic sequence (Fig. 7). It is observed that there is a good correlation between features on this surface and the gravity anomalies on the residual Bouguer gravity map.

The correlation confirms that the basement paleotopography developed during the rift phase controlled the formation of the evaporite basin (Kifumbi et al., 2017). The salt deposition evolved from the depocenters to the peripheral areas of the main gravimetric lows. The geometry of the gravimetric lows shows the geometry of the depocenters: the first depocenter is elongated in the SW-NE direction, corresponding to the Fazenda Guindaste Low (Martins et al., 2019), and the second is located to the west and presents a squared shape with the major axis trending NW-SE. To the east, there is an elongated structural high trending NE-SW, named Alagoas Hinge, which divides the coastal basin from the offshore domains (Souza-Lima et al., 2021).

While the top of the Coqueiro Seco Formation presents a rough relief, highly compartmentalized, the interpreted surface of the top of the overlying Maceió Formation is significantly smoother. This contrast evidences the cessation of the tectonic activity after the deposition of the Coqueiro Seco Formation. The Maceió Formation was deposited in the thermal subsidence regime, and represents a sag phase (Caixeta et al., 2014; Kifumbi et al., 2017).

The analysis of the structural framework revealed that two fault systems affected the evaporitic sequence. The primary system consists of deep-seated, high-angle NE-trending normal faults related to the rifting phase. These faults controlled the geometry of grabens and horsts and created the accommodation space for the evaporite deposition (Kifumbi et al., 2017). Superimposed to this regional fabric, there is a younger fault system that comprises shallower listric and detachment faults rooted in the evaporitic beds. As discussed by previous works, these structures were caused by the halokinesis effect and are responsible for localized deformation, including the development of rollover anticlines, folds and listric faults (Martins et al., 2019) (Fig. 8).

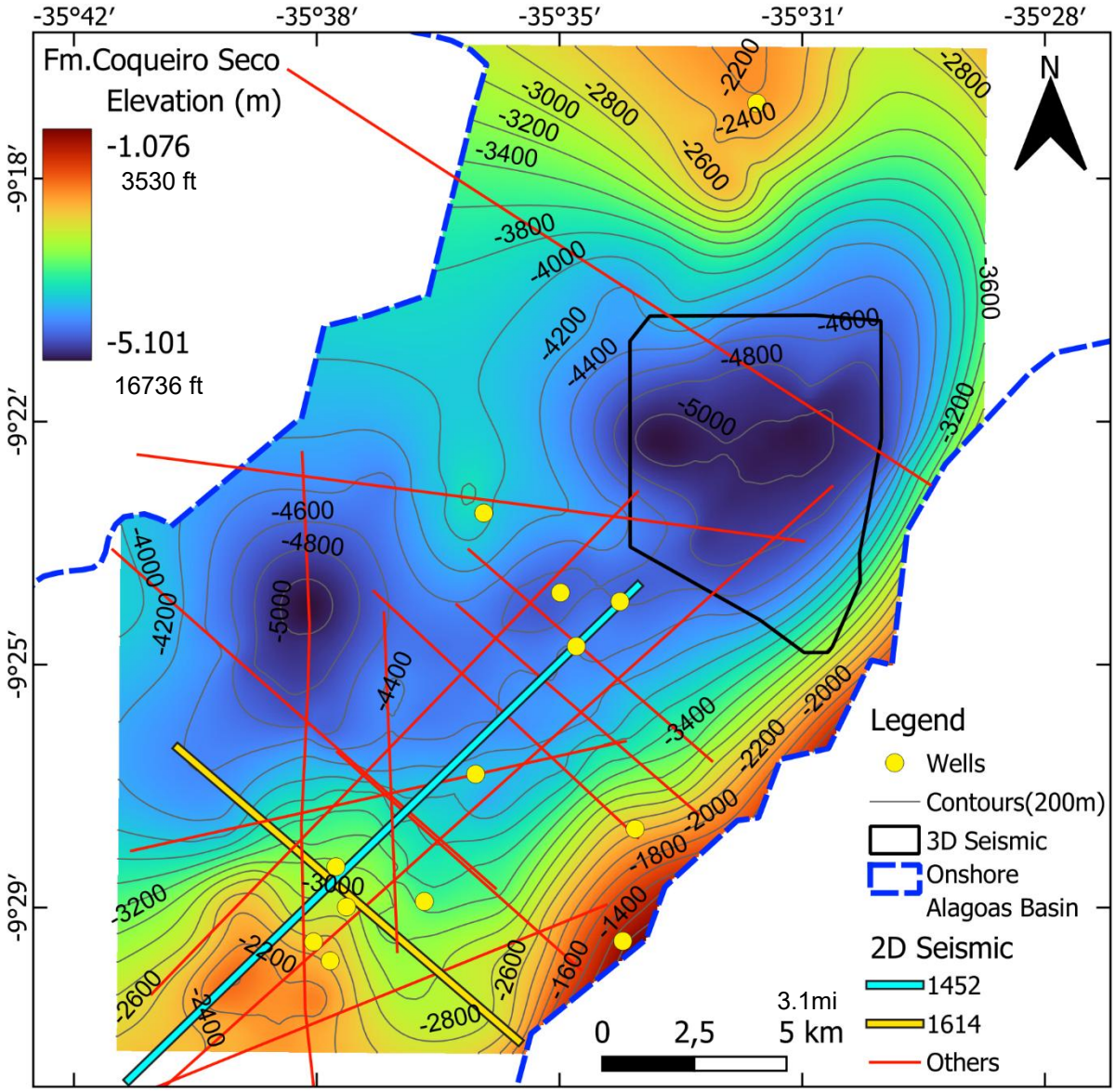

Fig. 7. Contour depth map of the top of the Coqueiro Seco (CQS) Formation, interpolated from well data (yellow dots), 2D (red lines), and 3D (black polygon) seismic data. The salt deposition was concentrated in the two major depocenters. The eastern border of the salt basin was formed by the external hinge. The seismic lines 1452 and 1614, which are respectively strike (SW-NE) and dip (NW-SE) oriented, are highlighted in the map and shown in the following Fig. 8. Below.

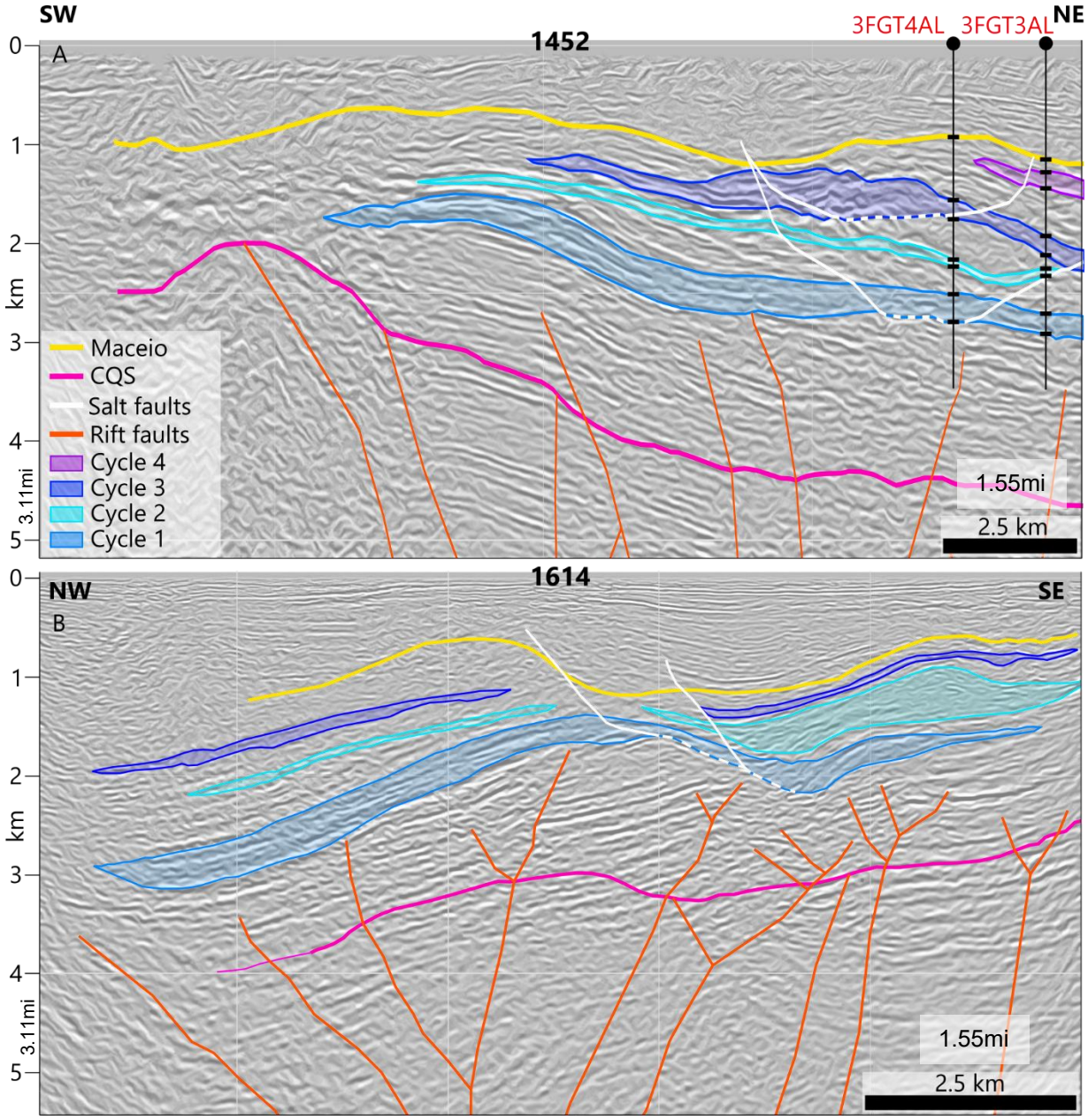

Fig. 8. 2D seismic sections showing the regional configuration of the evaporitic sequence within the Maceió Formation. A) Strike Section (top, SW-NE): This section shows the longitudinal section of the salt basin, characterized by the progressive thickening of the evaporitic cycles to the northeast and their pinch-out to the southwest. B) Dip Section (bottom, NW-SE): This section shows the interplay between rift faults and faults created by halokinesis. The image also shows the tilting of the strata towards the basin border (NW), and the division of the two depocenters created by a structural high.

4.2. Characterization of the Evaporitic Cycles

The analysis of the well logs allowed us to distinguish four depositional cycles within the Paripueira evaporites, named C1 to C4, from the oldest to the youngest. Each cycle is characterized by thick halite beds with interlayers, composed primarily of shales and carbonates, reflecting a depositional environment marked by high-frequency cyclic changes (Florencio, 2001).

The geometry and thickness of these cycles were heavily influenced by both the underlying rift topography and subsequent salt tectonics. Cycle C1 is the most laterally extensive and thickest in the sequence, with a maximum thickness of 665 m (2182 ft). Its relatively flat, continuous form, as shown on seismic sections, enabled it to serve as the main décollement level for the overlying halokinesis, with most salt-related listric faults terminating within this unit. After deposition, C1 experienced significant tilting toward both the northwest, in the direction of the border faults, and to the northeast.

In contrast, the geometries of C2 and C3 were controlled by a complex interplay between pre-existing rift faults and the deformation of the salt beds. This interaction caused localized folding that split the deposition of both C2 and C3 into a main depocenter in the central area and a smaller, secondary depocenter to the south, which contains the deposits referred to as Cycle C2b and Cycle C3b, respectively. The tilting of the strata that formed these cycles was controlled by the rift architecture, with beds of the C2 tilting towards the northwest and northeast, while strata from C3 tilts mainly to the northeast, reflecting the varying activity of the controlling faults during their deposition. Interpretation of the seismic data shows that these sub-basins, are bounded by listric faults and their associated rollover anticlines (Martins et al., 2019), and they provided the accommodation space for over 600 m (1968 ft) of deposits in cycle C2b (Fig. 11).

The C4 cycle, the youngest and less extensive in area, is primarily confined to the northeastern sector of the study area, where it reaches a maximum thickness of approximately 367 m (1204 ft). This spatial confinement is consistent with the northeastward tilt observed in the underlying cycles, suggesting that continued structural control exerted by the rift faults influenced the evolution of this late depocenter in this sector of the Fazenda Guindaste Low. Its shallower depth resulted in a lower overburden stress, which was less effective at developing the evaporite flow and deformation that characterized the deeper cycles, thus preserving a nearly horizontal geometry. The structural depth and the isopach maps for each of the four cycles are presented in Fig. 10 and 11, respectively. A critical characteristic of all cycles is the high frequency of insoluble interlayers (Florencio, 2001; Souza-Lima et al., 2019), which is consistently observed in well logs. The internal character of the cycles is observed in the well log analysis and is characterized by the rhythmic alternation of halite beds (low gamma-ray) and insoluble layers (high gamma-ray), (Fig. 9).

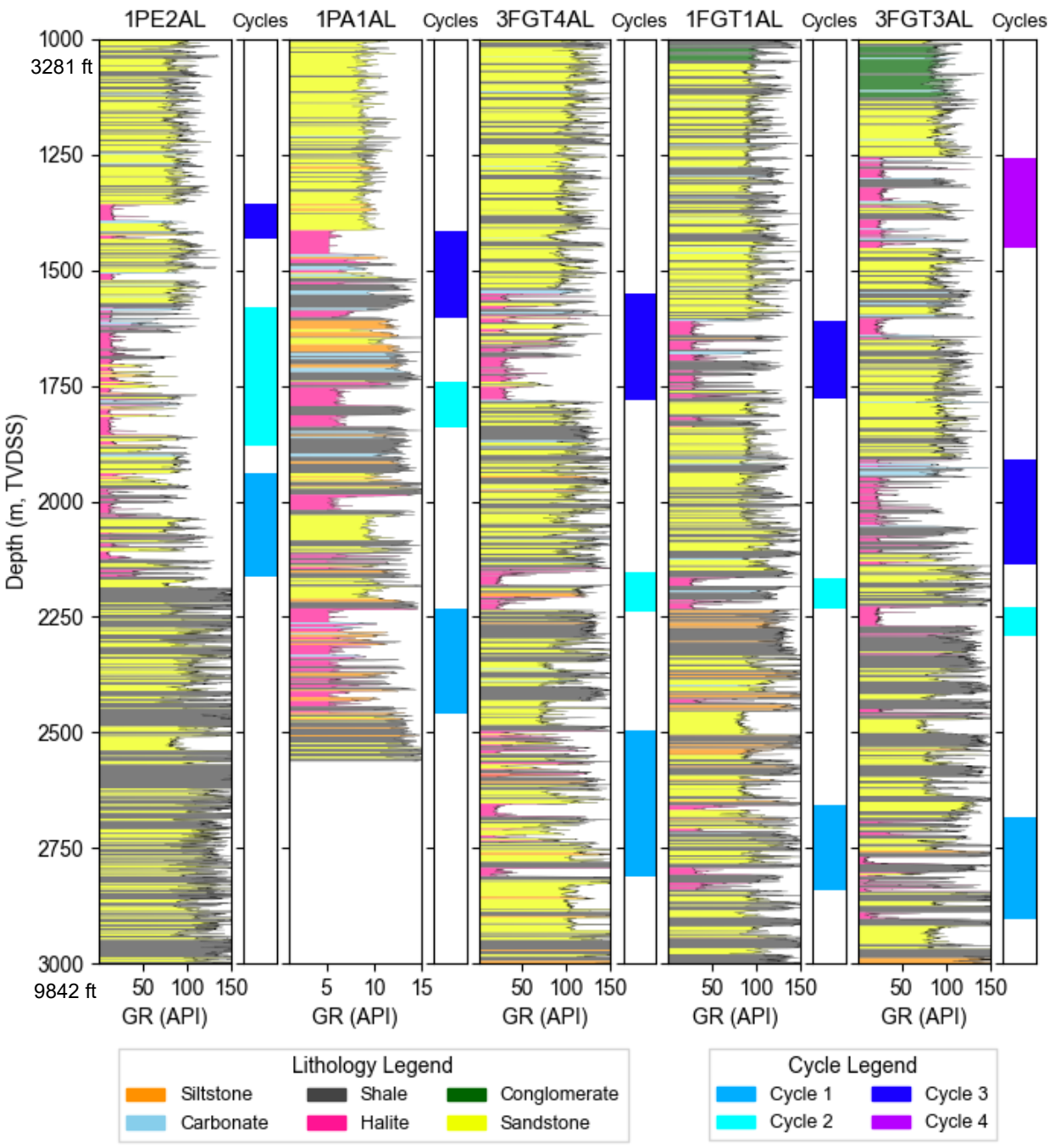

Fig. 9. Correlation of the Paripueira evaporites (1000-3000 m interval (3281-9842 ft)) based on gamma-ray (GR) logs from five wells (see location in Fig. 4). The GR profiles effectively discriminate clean halite (low values) from high-GR insoluble interlayers, enabling the correlation of four distinct evaporitic cycles. The section is displayed in True Vertical Depth Sub-Sea (TVDSS) to accurately represent the structural geometry of the deposits.

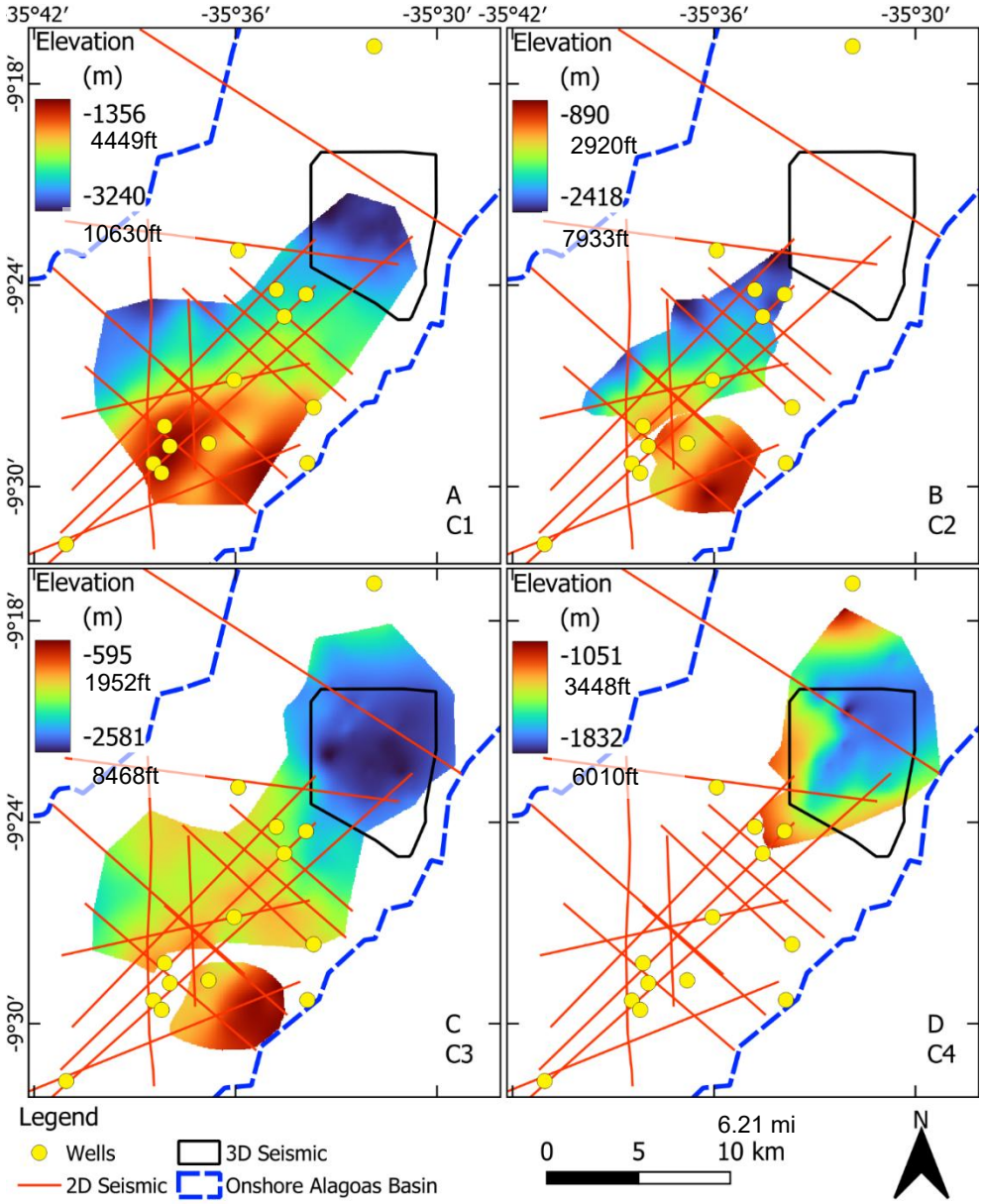

Fig. 10. Structural depth maps for the top of each of the four evaporitic cycles. The maps show the structural tilt deepening towards the NW and NE for Cycles C1 (A) and C2 (B) and towards the NE for Cycle C3 (C), while Cycle C4 (D) is restricted to the northeastern depocenter. The distinct southern depocenters for Cycles C2b and C3b (depth is TVDSS) are also highlighted.

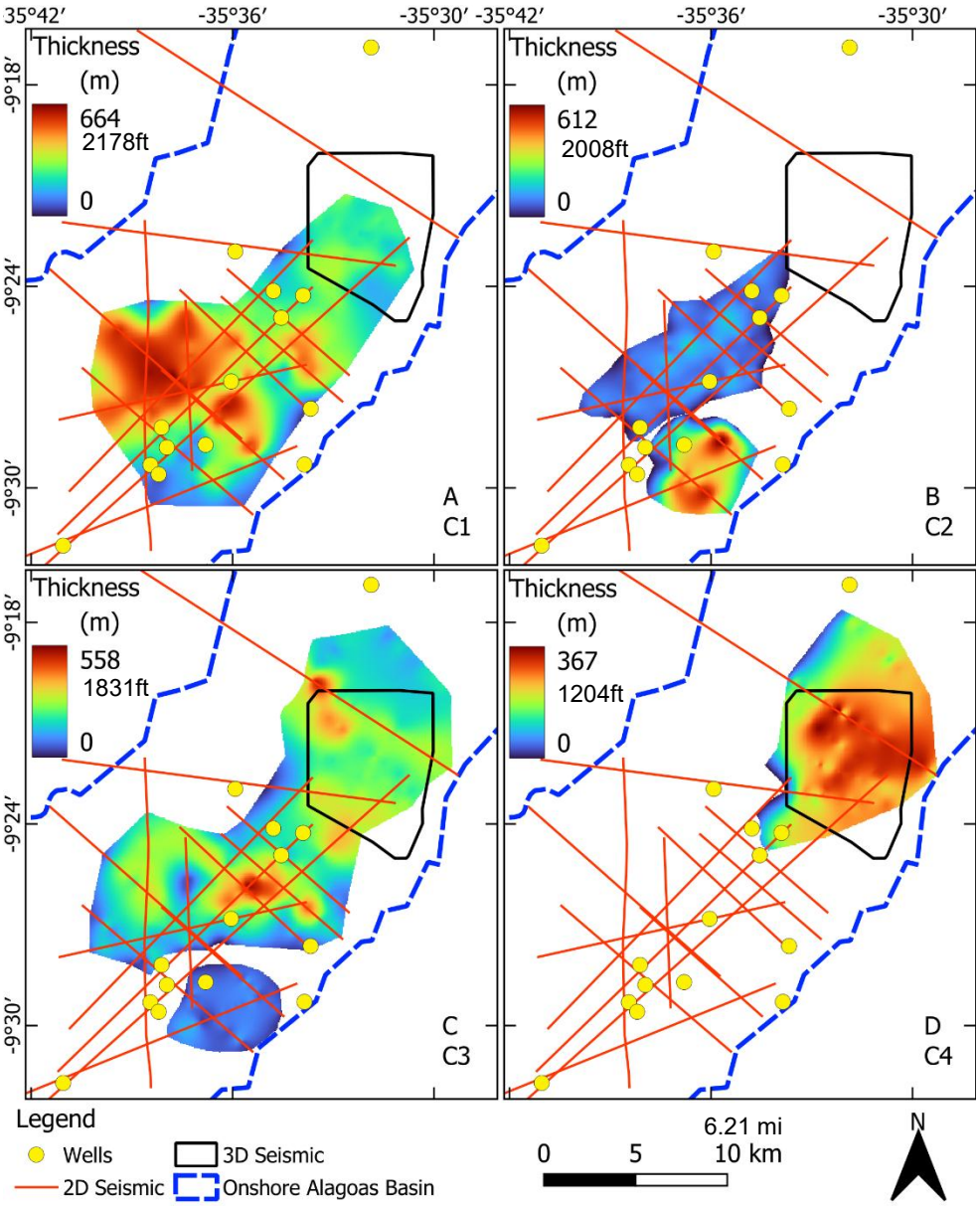

Fig. 11. Isopach maps of the four evaporitic cycles. The maps reveal a progressive confinement of deposition over time: Cycle 1 (A) shows widespread deposition, while Cycles C2 (B) and C3 (C) are compartmentalized into a primary northeastern depocenter and a secondary southern depocenter (C2b and C3b). For the Cycle C4 (D), the deposition was restricted to the main northeastern depocenter, highlighting the strong structural control on the sedimentation.

4.3. Favorability Mapping for UHS

A comprehensive favorability map for each evaporitic cycle was generated using a weighted overlay algorithm that synthesized all geometric and rock-property grids. The analysis effectively distinguished prospective zones from areas that were automatically designated as unviable. Extensive regions, particularly within Cycle C1 and the sub-cycle C3b, were excluded because they failed in one or more pre-defined hard cutoffs (Table 1). These thresholds represent critical safety and operational limits; any location failing to meet them was assigned a final favorability score of zero.

The favorability analysis process also identified zones with high favorability scores (score > 6.0) within Cycles C2b, C3, and C4. The most prospective areas include the central portion of Cycle C2b, a significant area in the central part of Cycle C3, and a zone in the central-east sector of Cycle C4. These "sweet spots" represent locations where the combination of sufficient thickness, adequate depth, favorable internal properties, and safe distance from faults offer safe volumes of salt rocks to be engineered. The final favorability maps for each cycle are shown on Fig. 12.

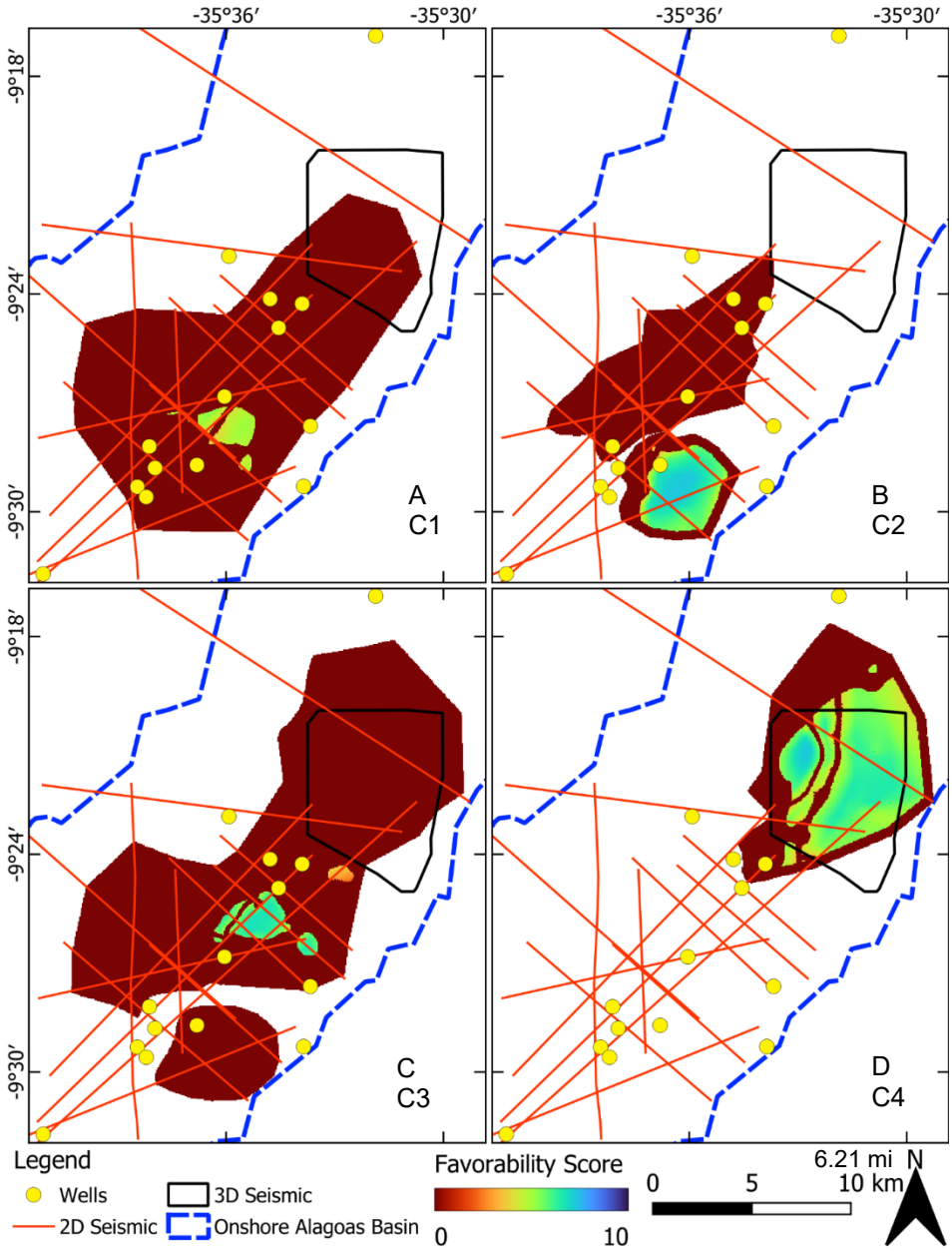

Fig. 12. Favorability maps for each evaporitic cycle. In three cycles most of the area was identified as inviable, and “sweet spots” were also located. Highly favorable zones are identified in the southern depocenter of Cycle C2 (B), a central area in Cycle C3 (C), and the central-east sector of Cycle C4 (D).

4.4. Hydrogen Storage Capacity Estimation

The final stage of the study assessed the region's storage potential based on a conceptual cavern field layout considering the favorable zones. The quantitative analysis provided a total effective energy storage

potential of approximately 13.5 TWh, which could be stored in a total of 237 caverns. This capacity is distributed in favorable zones, with Cycle C4 showing the largest potential (7.3 TWh from 118 caverns), followed by Cycle C2b (4.8 TWh from 81 caverns) and Cycle C3 (1.4 TWh from 38 caverns). A detailed breakdown of the allocated caverns and the estimated working gas mass and effective energy potential for each prospective cycle is presented in Table 2.

Table 2. Summary of the quantitative analysis of the storage **potential** in the favorable zones, from cavern allocation to effective energy capacity.

Cycle	No. of Allocated Caverns	Total Allocated Volume (m³)	Avg. Cavern Volume (m³/cavern)	Total Max H2 Mass (Kg)	Total Working H2 Mass (Kg)	Eff. Energy TWh	Avg. Eff. Energy per Cavern (GWh/cavern)
C2b	81	22,828,151 (806 MMcf)	281,829 (9.9 MMcf)	441,863,177 (974 MM lbs)	285,479,770 (629 MM lbs)	4.76	58.77
C3	38	6,101,173 (215 MMcf)	160,557 (5.7 MMcf)	130,456,796 (288 MM lbs)	84,754,495 (187 MM lbs)	1.41	37.11
C4	118	28,210,232 (996 MMcf)	239,070 (8.4 MMcf)	670,657,143 (1478 MM lbs)	439,224,612 (968 MM lbs)	7.32	62.03

A detailed layout of the caverns location was created for the most favorable zone within Cycle C2b, which included 81 individual caverns, considering geomechanical criteria for pillar stability (Fig. 13). This conceptual field alone demonstrates the potential to develop a large-scale storage hub.

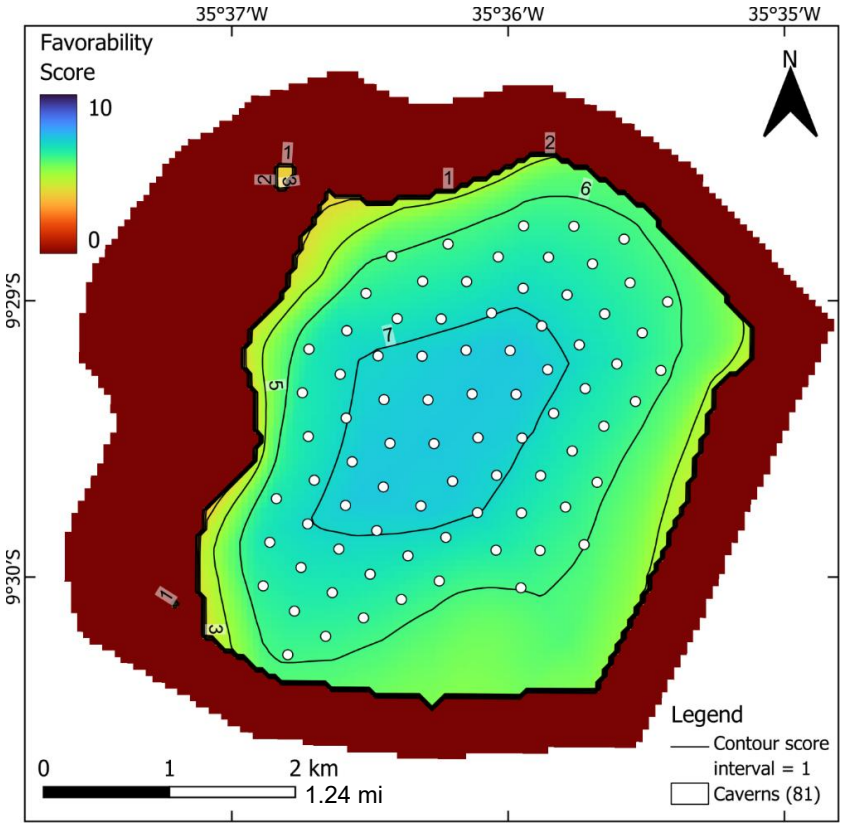

Fig. 13: Conceptual layout of a hydrogen storage hub constituted of isolated caverns (cavern diameter = 80m (262ft), pillar diameter = 240m (787ft)) within the most prospective zone of Cycle C2b. The map shows the systematic placement of 81 individual caverns (white circles) within the area of highest favorability (score > 6.0). This hub presents a potential capacity to store approximately 4.8 TWh of energy.

5. Discussion

5.1. Interpretation of Favorable Zones and Controlling Geological Factors

The results of the favorability analysis revealed a relationship between the salt beds´ thickness and tectono-stratigraphic constraints, which ultimately controlled the suitability of the Paripueira evaporites for Underground Hydrogen Storage (UHS). A key finding is that even the most promising areas do not achieve perfect scores, and the favorability index peaks at approximately 7.3 (Fig. 12). This maximum limit is a direct consequence of the inherent nature of this syn-rift evaporitic sequence, which is characterized by a high percentage of insolubles, a large number of interlayers, and expressive individual interlayer thickness in all cycles.

These factors penalize even the most favorable locations, highlighting the fact that the development of the region´s potential for UHS should consider the inherent challenges demonstrated here (Oni et al., 2025).

Cycle C1 serves as the best example of this aspect; although it represents the larger and thickest salt cycle, it was classified as largely non-favorable. Large exclusion zones within this cycle are linked to excessive depth and proximity of fault zones. This highlights that gross thickness alone is an insufficient indicator of suitability if we consider geomechanical risks (Allsop et al., 2023; Oni et al., 2025).

The most prospective zones, or "sweet spots," were therefore identified where a favorable conjunction of multiple geological parameters occurs in the younger cycles. Cycle 2, for instance, presents an inadequate thickness for viable cavern construction. However, in Cycle C2b the salt beds present a zone of high favorability. Cycle C3 has a large aerial extent in suitable depths, and large areas are penalized for having insufficient thickness, which negatively impacts both the thickness parameter and the potential cavern volume score; furthermore, it is cut by multiple halokinesis-related faults that create significant exclusion zones. The associated C3b cycle was entirely excluded, because the general thickness is mostly below the 100 m (328 ft) cutoff threshold. In contrast, Cycle C4 presents a more regular geometry, and it is within an adequate depth window. In this cycle, despite the favorability observed in the maps, a corridor of low favorability observed is the result of a restraining condition created by two salt-related faults.

A critical uncertainty that must be highlighted is that the high-favorability assessments for the promising zones within Cycle C2b and Cycle C4 are dependent on rock property data extrapolated from a single well in each area. This reliance on a sparse legacy dataset is a well-known source of uncertainty in regional geological modeling (Allsop et al., 2023). However, there is a key distinction in the confidence level between these two zones. The assessment of Cycle C4 is supported by the interpretation of a 3D seismic volume, which provides the best data of the structural framework and stratigraphic continuity. Furthermore, the characterization of Cycle C2b relies on a sparse grid of 2D seismic sections, resulting in greater uncertainties. This distinction can guide the recommendations for future work, emphasizing new data acquisition to de-risk promising but insufficiently surveyed areas.

5.2. Geomechanical Context and Analogues

The geomechanical challenges identified in this study, particularly the high frequency of insoluble interlayers and the complex deformation associated with halokinesis, are characteristic of syn-rift bedded salt deposits worldwide (Martins et al., 2019; Oni et al., 2025). Unlike the thick, homogenous salt domes often favored for UHS, bedded salt formations require a more rigorous geomechanical assessment due to the mechanical contrast between the ductile halite and the more brittle interlayers composed of shales, carbonates, and shaly siltstones (Zhang et al., 2017). During cavern operation, cyclic loading can induce stress concentration at the salt-interlayer interfaces, potentially leading to micro-fracturing, loss of sealing effect, and long-term stability issues (Oni et al., 2025). The long history of solution mining in the nearby Maceió area can also be used as a proximal analogue that highlights the critical importance of understanding and mitigating geomechanical risks to prevent surface subsidence and ensure operational integrity and safety.

Global experience corroborates the challenges identified. Projects in bedded salt, such as in China and parts of the US, have demonstrated that while UHS is feasible, it demands meticulous cavern design to manage the risks posed by geological heterogeneity (Zhang et al., 2017; Duartey et al., 2025). The presence of numerous, and sometimes thick, interlayers within the Paripueira evaporites (Fig. 9) is a

significant concern, as these layers can lead to irregular cavern shapes during leaching and act as preferential pathways for hydrogen leakage if their integrity is compromised (Oni et al., 2025). The salt's creep behavior, which leads to cavern convergence over time, represents another critical factor that must be managed by maintaining a minimum operating pressure, a standard practice in the industry (Allsop et al., 2023). Therefore, while the Alagoas Basin holds significant potential, its development must be critically analyzed against these international analogues, which can help to ensure best practices for characterization and engineering in geologically complex bedded salt.

5.3. Key Uncertainties and Operational Risks

The favorability approach presented in this study provides a robust regional screening tool, but it is inherently subject to uncertainties dependent on the quality of the legacy dataset. The spatial distribution of well data is sparse, and the 2D seismic sections provide limited three-dimensional coverage on the complex geometry of faults and salt bodies (Allsop et al., 2023). This leads to a higher degree of uncertainty in aspects like the distribution of rock properties, such as the percentage of insolubles and the thickness of interlayers, in areas distant from the available wells. Consequently, the boundaries of the favorable zones should be considered indicative rather than absolute, requiring confirmation through further acquisition of higher-resolution data.

The primary operational risk identified is the integrity of the storage system due to the high frequency of interlayers (Florencio, 2001; Souza-Lima et al., 2019). While the well data confirmed the presence of shales and carbonates, the potential for more permeable lithologies like sandstones within the interbedded sequences cannot be discounted and represents a significant risk to cavern tightness (Florencio, 2001; Oni et al., 2025). Hydrogen, due to its small molecular size and low viscosity, can permeate through materials and microfractures more readily than natural gas, making the cavern sealing capacity the critical factor for UHS (Duartey et al., 2025). The suggested cavern field layout (Fig. 13) represents a tentative verification of the storage capacity; to achieve effective guidance it is necessary to improve the exploratory data and to perform coupled geomechanical and chemical studies. These simulations must model the thermo-mechanical effects of high-frequency injection and withdrawal cycles and their long-term impact on the stability of both the salt structures and the interlayers to ensure a safe and efficient operational lifespan of 30 to 50 years (Allsop et al., 2023; Oni et al., 2025).

5.4. Strategic Implications for a Hydrogen Hub in NE Brazil

The confirmation of a potential storage capacity of at least 13.5 TWh positions the Alagoas Basin as a strategic asset for anchoring a large-scale green hydrogen hub in northeastern Brazil. This region possesses some of the world's highest quality wind and solar resources, making it a prime candidate for globally competitive green hydrogen production (Rocha et al., 2012; Anjos et al., 2024). Furthermore, the geographical location of the favorable zones offers significant logistical and strategic advantages. The sites are situated in a rural area 15 to 30 km (9.3 to 18.6 mi) north of the Maceió urban center, minimizing potential land-use conflicts and public safety concerns while remaining in close proximity to essential infrastructure, including ports for potential hydrogen exports (e.g., ammonia) and a well-developed road network. The region is also characterized by low seismic risk and has access to the water resources required for the solution mining process, further strengthening its strategic value. By de-risking the subsurface storage component, this study provides a critical piece of the puzzle, enhancing the attractiveness of Alagoas Basin for the significant international investments flowing into the global hydrogen economy (Anjos et al., 2024).

5.5. Recommendations for Future Work

To mature the identified potential and transition from a regional assessment to a project-level evaluation, future work should focus on reducing the key uncertainties — namely the reliance on low-resolution legacy data and sparse well distribution — through a phased and targeted approach. Based on the findings of this study, the following integrated steps are suggested:

- **High-Resolution 3D Seismic Acquisition:** A new 3D seismic survey should be acquired, with priority on the highly favorable depocenter of Cycle C2b, to accurately map complex fault networks

and characterize the continuity of internal interlayers, which are poorly resolved by the existing legacy data.

- **Targeted Drilling and Site Investigation:** A drilling campaign in the identified 'sweet spots' is crucial for direct data acquisition. This would involve extensive coring and sampling for detailed laboratory and in-situ geomechanical testing (e.g., creep parameters, leak-off tests) and a comprehensive geochemical risk assessment. This assessment must evaluate not only biogeochemical risks, such as microbially induced souring (H_2S production), but also potential abiotic (inorganic) reactions between the stored hydrogen, brine, and reactive minerals in the interlayers.
- **Integrated Modeling and Engineering Design:** The new dataset would enable the construction of calibrated geomechanical and cavern engineering models. These models are essential to simulate the full operational life cycle and optimize cavern design and field layout to ensure long-term mechanical stability and operational safety.
- **Techno-Economic and Socio-Environmental Assessment:** Finally, a comprehensive study is needed to assess the techno-economic viability of establishing a hydrogen hub in Alagoas and evaluate potential socio-environmental impacts, such as predicted surface subsidence, ensuring a sustainable and socially responsible project design.

6. Conclusion

This study presents the first systematic, data-driven assessment of the Aptian Paripueira evaporites in the onshore Alagoas Basin, NE Brazil, for UHS. By integrating a legacy dataset of well logs, 2D/3D seismic data, and gravity data into a comprehensive 3D tectono-stratigraphic model, this work successfully applied a quantitative de-risking tool to achieve a comprehensive appraisal of the feasibility of storing hydrogen in this evaporitic succession. The application of a multi-criteria favorability algorithm delineated specific prospective zones, or "sweet spots," within the complex syn-rift evaporitic sequence.

The Paripueira evaporites are characterized by a complex structural framework, a product of rift-related faulting and subsequent halokinesis, and a high frequency of insoluble interlayers. These geological complexities, which are inherent to the syn-rift nature of the deposits, impose critical constraints on cavern stability and integrity. Our analysis revealed a significant storage potential, with a quantitative assessment indicating that the most favorable zones could support the development of a cavern field with a total effective energy potential estimated at approximately 13.5 TWh. This represents the net electrical energy that could be cyclically generated from the stored working hydrogen, assuming a power conversion efficiency of 50%. This capacity is primarily concentrated in three distinct units: the southern depocenter of Cycle C2, the central area of Cycle C3, and, most notably, the central-east sector of Cycle C4. These findings strategically position the Alagoas Basin as a strong candidate for establishing a large-scale energy hub, a critical step for realizing Brazil's potential to become a key player in the global green hydrogen economy.

However, the study also highlights that for the realization of this potential it is critical to predict and avoid significant geomechanical challenges. Therefore, while this investigation confirms a substantial opportunity based on the available data, it concludes that future development must be guided by new detailed geological and geophysical investigations. These should include high-resolution 3D seismic acquisition and targeted drilling campaigns focused on rigorous geomechanical testing to ensure the safe and reliable long-term operation of any future UHS facility.

Acknowledgements

The authors would like to thank the National Agency for Petroleum, Natural Gas and Biofuels (ANP) and the Geological Survey of Brazil (SGB) for providing the geological and geophysical data used in this study, made available through the REATE Project (Terrestrial Basin Reassessment Project). A. Barbosa acknowledges the financial support from CNPq, grant number 312294/2023-9.

Appendix A. Virial Coefficients for Hydrogen Compressibility

The following table details the virial coefficients used in the standardized virial-type equation of state (Equation 5 in the main text) for the calculation of the hydrogen compressibility factor (Z). These constants are sourced from the work of Lemmon, Huber, and Leachman (2008).

Table A.1. Constants for the virial-type equation for hydrogen density, as presented by Lemmon et al. (2008).

i	Ai	Bi	Ci
1	0.0588846	1.325	1.000
2	-0.06136111	1.870	1.000
3	-0.002650473	2.500	2.000
4	0.002731125	2.800	2.000
5	0.001802374	2.938	2.420
6	-0.001150707	3.140	2.630
7	9.588528E-05	3.370	3.000
8	-1.109040E-07	3.750	4.000
9	1.264403E-10	4.000	5.000

References

Allsop, C., Yfantis, G., Passaris, E., Edlmann, K., 2023. Utilizing publicly available datasets for identifying offshore salt strata and developing salt caverns for hydrogen storage. In: Miocic, J.M., Heinemann, N., Edlmann, K., Alcalde, J., Schultz, R.A. (Eds.), Enabling Secure Subsurface Storage in Future Energy Systems. Geological Society, London, Special Publications, 528, pp. 139-169. https://doi.org/10.6084/m9.figshare.c.6315742.v2

Anjos, K.C.D. dos, et al., 2024. Renewable energy in the brazilian northeast: challenges and opportunities. Contribuciones a Las Ciencias Sociales 17 (6), 1-19. https://doi.org/10.55905/revconv.17n.6-177.

ANP - Agência Nacional do Petróleo, Gás Natural e Biocombustíveis, 2023. Public data from the REATE Project (Projeto de Reavaliação das Bacias Terrestres). Available at: http://reate.cprm.gov.br/anp. Accessed: 18 August 2025.

Argollo, R.M., Marinho, M.M., Costa, A.B., Sampaio Filho, H.A., Santos, E.J., Coutinho, L.F.C., 2012. Crustal model and heat flow in the Estância, Canudos-Vaza-Barris and Macururé domains bordering the emerged edge of Sergipe-Alagoas Basin (Modelo crustal e fluxo de calor nos domínios Estância, Canudos-Vaza-Barris e Macururé adjacentes às bordas emersas da Bacia Sergipe-Alagoas). *Boletim de Geociências da Petrobras* 20(1/2), 283–304. (in Portuguese).

Caglayan, D.G., Weber, N., Heinrichs, H.U., Linßen, J., Robinius, M., Kukla, P.A., Stolten, D., 2020. Technical potential of salt caverns for hydrogen storage in Europe. *International Journal of Hydrogen Energy* 45(11), 6793-6805. https://doi.org/10.1016/j.ijhydene.2019.12.161

Caixeta, J.M., et al., 2014. Albian Rift Systems in the Northeastern Brazilian Margin: An Example of Rifting in Hyper-Extended Continental Crust. AAPG Search and Discovery, Article #30378.

Campos Neto, O.A., Souza Lima, W., Cruz, F.E.G., Feijó, F.J., 2007. Bacia de Sergipe-Alagoas. *Boletim de Geociências da Petrobras* 15(2), 427-437.

Cruz, F.E.G., 2008. Arcabouço Estrutural e Tectônica Salífera da Bacia de Sergipe-Alagoas. In: Mohriak, W.U., Szatmari, P., Anjos, S.M.C. (Eds.), Sal: Geologia e Tectônica. Beca, São Paulo, pp. 264-283.

Duartey, K.O., Ampomah, W., Rahnema, H., Mehana, M., 2025. Underground Hydrogen Storage: Transforming Subsurface Science into Sustainable Energy Solutions. *Energies* 18(3), 748. https://doi.org/10.3390/en18030748

Florencio, C.P., 2001. A Tectônica Salífera Aptiana da Bacia de Sergipe-Alagoas: Evolução e Influência na Sedimentação Pós-Sal. Ph.D. Thesis, Universidade Federal de Ouro Preto, Ouro Preto, Brazil.

Harrison, K.W., Remick, R., Martin, G.D., Hoskin, A., 2010. Hydrogen Production: Fundamentals and Case Study Summaries. Conference Paper NREL/CP-550-47302. Presented at the 18th World Hydrogen Energy Conference, Essen, Germany. National Renewable Energy Laboratory, Golden, CO.

Huang, J., Yin, S., 2025. Optimization of the design of underground hydrogen storage in salt caverns in Southern Ontario, Canada. Mining 5, 9. https://doi.org/10.3390/mining5010009.

Kifumbi, C., Scherer, C.M.S., Jones, F.H., Kuchle, J., 2017. High resolution stratigraphy of initial stages of rifting, Sergipe-Alagoas Basin, Brazil. Braz. J. Geol. 47 (4), 657-671. https://doi.org/10.1590/2317-4889201720170003.

Lemmon, E.W., Huber, M.L., Leachman, J.W., 2008. Revised Standardized Equation for Hydrogen Gas Densities for Fuel Consumption Applications. *Journal of Research of the National Institute of Standards and Technology* 113(6), 341–350. https://doi.org/10.6028/jres.113.028

Liu, W., Dong, Y., Zhang, Z., Li, L., Jiang, D., Fan, J., Chen, J., Zhang, X., Wan, J., Li, Z., 2024. Optimization of operating pressure of hydrogen storage salt cavern in bedded salt rock with multi-interlayers. *International Journal of Hydrogen Energy* 58, 974–986. https://doi.org/10.1016/j.ijhydene.2024.01.318

Martins, M.V.A., 2016. Os evaporitos das Formações Coqueiro Seco (Horizonte Evaporítico) e Maceió (Paripueira Evaporitos) na porção terrestre da Bacia de Alagoas. Master's Thesis, Universidade do Estado do Rio de Janeiro, Rio de Janeiro, Brazil.

Martins, M.V.A., Souza-Lima, W., Barbosa, J.A., 2019. Aptian halokinesis in the onshore portion of the Alagoas basin, northeastern Brazil (Halocinese aptiana na porção emersa da bacia de Alagoas, nordeste do Brasil). *Geociências* 38(1), 209-222. (in Portuguese).

Medeiros, V.C., Medeiros, W.E., Jardim de Sá, E.F., 2006. Contribution of Gravimetry to the Definition of the Regional Tectonic Framework of the Sergipe-Alagoas Basin (Contribuição da Gravimetria para a Definição do Arcabouço Tectônico Regional da Bacia Sergipe-Alagoas). In: Proceedings of the 43rd Brazilian Geological Congress, Aracaju. Annals... Sociedade Brasileira de Geologia, Aracaju. (in Portuguese).

Oni, B.A., Bade, S.O., Sanni, S.E., Orodu, O.D., 2025. Underground hydrogen storage in salt caverns: Recent advances, modeling approaches, barriers, and future outlook. J. Energy Storage 107, 114951. https://doi.org/10.1016/j.est.2024.114951.

Rocha, K., Gutierrez, M.B.G.P.S., Hauser, P., 2012. A remuneração dos investimentos em energia renovável no Brasil - uma proposta metodológica ao benchmark da UNFCCC para o Brasil. Texto para Discussão, 1701, Instituto de Pesquisa Econômica Aplicada (IPEA), Rio de Janeiro. Available at: https://www.ipea.gov.br/portal/images/stories/PDFs/TDs/td_1701.pdf. (Accessed 19 August 2025).

Souza-Lima, W., 2008. Bacias de Sergipe e Alagoas. In: Milani, E.J., Rangel, A.P., Bueno, G.V., Stica, J.M., Winter, W.R., Caixeta, J.M., Faria, L.C. (Eds.), Bacias Sedimentares Brasileiras: Cartas Estratigráficas. *Boletim de Geociências da Petrobras* 16(1), 181-197.

Souza-Lima, W., Andrade, E.J., Santos, P.R., Coqueiro, E.S., 2019. Revisão litoestratigráfica da seção cretácea aflorante no norte do estado de Alagoas e sul de Pernambuco, bacias de Alagoas e Pernambuco. *Geociências* 38(1), 223–236.

Souza-Lima, W., Pierini, C., Fischer, C.M., Silva, B.O., 2021. Cretaceous late aptian paleogeography from northeastern Sergipe-Alagoas Basin, Brazil. Geociências (São Paulo) 40 (2), 397-406. https://doi.org/10.5016/geociencias.v40i02.15394.

Xia, C., Zhou, Y., Zhou, S., Zhang, P., Wang, F., 2015. A simplified and unified analytical solution for temperature and pressure variations in compressed air energy storage caverns. Renew. Energy 74, 718-726. https://doi.org/10.1016/j.renene.2014.08.058.

Yu, H., Liu, Y., Ma, H., Zhao, K., Liu, J., 2022. Pillar safety in shallow salt caverns by using numerical simulations. J. Energy Storage 55, 105881. https://doi.org/10.1016/j.est.2022.105881.

Zhang, N., Ma, L., Wang, M., Zhang, Q., Li, J., Fan, P., 2017. Comprehensive risk evaluation of underground energy storage caverns in bedded rock salt. *Journal of Loss Prevention in the Process Industries* 45, 264–276. https://doi.org/10.1016/j.jlp.2016.10.016

Zhu, S., Shi, X., Yang, C., Bai, W., Wei, X., Yang, K., Li, P., Li, H., Li, Y., Wang, G., 2024. Site selection evaluation for salt cavern hydrogen storage in China. Renew. Energy 224, 120143. https://doi.org/10.1016/j.renene.2024.120143.